Monthly Notices
of the
ROYAL ASTRONOMICAL SOCIETY

Mon. Not. R. Astron. Soc. **418,** 2493–2507 (2011) doi:10.1111/j.1365-2966.2011.19640.x

Rigging dark haloes: why is hierarchical galaxy formation consistent with the inside-out build-up of thin discs?

C. Pichon,[1,2,3⋆] D. Pogosyan,[4] T. Kimm,[2] A. Slyz,[2] J. Devriendt[2,3] and Y. Dubois[2]

[1]*Institut d'Astrophysique de Paris, 98 bis boulevard Arago, 75014 Paris, France*
[2]*Department of Astrophysics, University of Oxford, Keble Road, Oxford OX1 3RH*
[3]*Observatoire de Lyon (UMR 5574), 9 avenue Charles André, F-69561 Saint Genis Laval, France*
[4]*Department of Physics, University of Alberta, 11322-89 Avenue, Edmonton, Alberta T6G 2G7, Canada*

Accepted 2011 August 15. Received 2011 July 27; in original form 2011 May 1

ABSTRACT

State-of-the-art hydrodynamical simulations show that gas inflow through the virial sphere of dark matter haloes is focused (i.e. has a preferred inflow direction), consistent (i.e. its orientation is steady in time) and amplified (i.e. the amplitude of its advected specific angular momentum increases with time). We explain this to be a consequence of the dynamics of the cosmic web within the neighbourhood of the halo, which produces steady, angular momentum rich, filamentary inflow of cold gas. On large scales, the dynamics within neighbouring patches drives matter out of the surrounding voids, into walls and filaments before it finally gets accreted on to virialized dark matter haloes. As these walls/filaments constitute the boundaries of asymmetric voids, they acquire a net transverse motion, which explains the angular momentum rich nature of the later infall which comes from further away. We conjecture that this large-scale driven consistency explains why cold flows are so efficient at building up high-redshift thin discs inside out.

Key words: galaxies: evolution – galaxies: formation – galaxies: kinematics and dynamics – galaxies: statistics – galaxies: structure – large-scale structure of Universe.

1 INTRODUCTION

One of the persistent puzzles of the standard paradigm of galaxy formation is the following: why do we observe *thin* galactic discs when hierarchical clustering naively suggests that these galaxies should undergo repetitive random interactions with satellites and incoherent gas infall from their environment? Indeed whilst one can argue that the probability of a head-on collision with satellites should be small, incoherent but continuous gas infall poses a much greater threat to the ability of a bottom-up scenario of galaxy formation to form ubiquitous thin galactic discs. Historically, astronomers (Rees & Ostriker 1977; Silk 1977) have invoked the primordial monolithic collapse of a spheroidal body of gas which is shock-heated to its virial temperature. In this scenario, subsequent in-falling gas (Fillmore & Goldreich 1984; Bertschinger 1985, now described as secondary infall) shock-heats as it hits the virial radius, while the inner, denser region of the hot gaseous sphere secularly rains on to the central disc as it radiatively cools. This process has been named the 'hot mode' of gas accretion and implies a clear correlation between the spin of the hot galactic corona and that of the disc which is effectively assumed to be shielded from its cosmic environment (Fall & Efstathiou 1980; Mo, Mao & White 1998; Bullock et al. 2001).

Over the last few years it has been (re)realized (Birnboim & Dekel 2003; Kereš et al. 2005; Ocvirk, Pichon & Teyssier 2008; Brooks et al. 2009; Dekel et al. 2009) that most of the gas-feeding galaxies arrive cold ($\approx 10^4$ K) from the large-scale structures along filaments, and does not create such a halo-filling corona of hot gas, as the radiative shock it must necessarily generate to do so is unstable to cooling processes. These investigations correspond to an update in the current Lambda cold dark matter (ΛCDM) cosmological framework of the basic prediction of Binney (1977) who argued that for all but the most massive galaxies, the accreted gas, provided it was dense enough, would never shock-heat to temperatures where Bremsstrahlung dominates cooling as it would first cool by atomic transitions. In the author's own words, the accretion shock would be 'isothermal' rather than 'adiabatic' and, consequently, only a negligible fraction of the gas would ever reach temperatures $T \sim T_{\rm vir}$. In parallel to the work of Aubert, Pichon & Colombi (2004) on anisotropic *dark matter* infall on to galactic haloes, Katz et al. (2003) and Kereš et al. (2005) numerically confirmed that a large fraction of the gas is indeed accreted through filamentary streams, where it remains cold before it reaches the galaxy (see also Kay et al. 2000; Fardal et al. 2001 for reports on the early indication that this gas was not shock-heated). This 'cold-mode' accretion dominates

⋆E-mail: pichon@iap.fr

the global growth of all galaxies at high redshifts ($z \geq 3$) and the growth of low-mass ($M_{\rm halo} \leq 5 \times 10^{11}\,{\rm M}_{\odot}$) objects at late times (Dekel & Birnboim 2006).

The addition of accretion through cold streams to the standard galaxy formation framework has received much attention (e.g. Brooks et al. 2009; Kereš et al. 2009) because of its potential implications for the star formation history of galaxies (however, see Benson & Bower 2011 for a defense of the opposite point of view). In the traditional 'hot mode' picture, star formation is delayed as accreted gas is shock heated and requires time to cool on to the central object. In contrast, if this material comes in cold, star formation can be fuelled on a halo free-fall time. Cold-mode accretion should also have an important impact on the properties (scalelength, scaleheight, rotational velocity) of galactic discs if, as conjectured by Kereš et al. (2005), cold streams merge on to discs 'like streams of cars entering an expressway', converting a significant fraction of their infall velocity to rotational velocity. Dekel et al. (2009) argued along the same lines in their analysis with the HORIZON-MareNostrum simulation: the stream carrying the largest coherent flux with an impact parameter of a few kiloparsecs may determine the disc's spin and orientation. Powell, Slyz & Devriendt (2011) spectacularly confirmed these conjectures by showing that indeed, the filaments connect rather smoothly to the disc: they appear to join from different directions, coiling around one another and forming a thin extended disc structure, their high velocities driving its rotation.

The way angular momentum is advected through the virial sphere as a function of time is expected to play a key role in rearranging the gas and dark matter within dark matter haloes. The pioneering works of Peebles (1969); Doroshkevich (1970); White (1984) addressed the issue of the original spin-up of collapsed haloes, explaining its linear growth up to the time the initial overdensity decouples from the expansion of the Universe through the realignment of the primordial perturbation's inertial tensor with the shear tensor. However, little theoretical work has been devoted to analysing the outskirts of the Lagrangian patches associated with virialized dark matter haloes, which account for the later infall of gas and dark matter on to the already formed haloes. In this paper, we quantify how significant this issue is and present a consistent picture of the time evolution of angular momentum accretion at the virial sphere based on our current theoretical understanding of the large-scale-structure dynamics. More specifically, the paper presents a possible answer to the conundrum of why cold gas flows in ΛCDM universes are consistent with thin disc formation. Indeed, as far as galactic disc formation is concerned, the heart of the matter lies in understanding how and when gas is accreted through the virial sphere on to the disc. In other words, what are the geometry and temporal evolution of the gas accretion?

In the 'standard' paradigm of disc formation, this question was split into two. Both the dark matter and gas present in the virialized halo acquired angular momentum through tidal torques in the pre-virialization stage, i.e. until turnaround (e.g White 1984). The gas was later shock-heated as it collapsed, and secularly cooled and condensed into a disc (Fall & Efstathiou 1980) having lost most of the connection with its anisotropic cosmic past. In the modern cold-mode accretion picture which now seems to dominate all but the most massive haloes, these questions need to be re-addressed. This paper presents a new scenario in which the coherence in the disc build-up stems from the orderly motion of the filamentary inflow of cold gas coming from the outskirts of the collapsing galactic patch. The outline is as follows. In Section 2, using hydrodynamical simulations, we report evidence that filamentary flows advect an ever-increasing amount of angular momentum through the halo virial sphere at redshifts higher than 1.5. We also demonstrate that the orientation of these flows is consistent, i.e. maintained over long periods of time. Section 3 presents results obtained through simplified pure dark matter simulations of the collapse of a Lagrangian patch associated with a virialized halo as these have the merit of better illustrating the dynamics of matter flows on the outskirts of the halo. Section 4 is devoted to the presentation of the conjectured impact of this scenario on disc growth at various redshifts, conclusions and prospects.

2 HYDRODYNAMICAL EVIDENCE

Let us start by briefly reporting the relevant hydrodynamical results we have obtained. We statistically analysed the advected specific angular momentum of both gas and dark matter at the virial radius of dark haloes in the HORIZON-MareNostrum cosmological simulation at redshift 6.1, 5.0, 3.8, 2.5 and 1.5 (see Figs 1 and 2 details can be found in Kimm et al. 2011).

The HORIZON-MareNostrum simulation (Ocvirk et al. 2008; Devriendt et al. 2010) was carried out using the Eulerian hydrodynamic code, RAMSES (Teyssier 2002), which uses an adaptive mesh refinement (AMR) technique. It followed the evolution of a cubic cosmological volume of $50\,{\rm h}^{-1}\,{\rm Mpc}$ on a side (comoving), containing 1024^3 dark matter particles and an Eulerian root grid of 1024^3 gas cells. A ΛCDM concordance universe ($\Omega_{\rm m} = 0.3$, $\Omega_{\Lambda} = 0.7$, $\Omega_{\rm b} = 0.045$, $h = H_0/(100\,{\rm km\,s^{-1}\,Mpc^{-1}}) = 0.7$, $\sigma_8 = 0.9$, $n = 1$) corresponding to the *WMAP* 1 best-fitting cosmology was adopted, resulting in a dark matter particle mass $m_{\rm p} = 1.41 \times 10^7\,{\rm M}_{\odot}$. A quasi-Lagrangian refinement policy was enforced to keep the spatial resolution fixed at about $1\,h^{-1}\,{\rm kpc}$ in physical coordinates. A uniform ultraviolet (UV) background instantaneously turned on at $z = 8.5$ was adopted (Haardt & Madau 1996). Gas was allowed to radiatively cool (Sutherland & Dopita 1993) and sink in the potential well of DM haloes. Whenever the gas exceeded the threshold density of $n_{\rm H} = 0.1\,{\rm cm^{-3}}$, 5 per cent of it turned into stars per local free-fall time. Massive young stars exploded as supernova after a time delay of 10 Myr corresponding to their average lifetime, and we modelled these explosions using a Sedov blast wave solution (Dubois & Teyssier 2008). Cooling enhancement down to $10^4\,{\rm K}$ due to the presence of metals is considered in the HORIZON-MareNostrum simulation. Potentially important physics such as active galactic nucleus (AGN) feedback, magnetic fields and radiative transfer were ignored in the simulation.

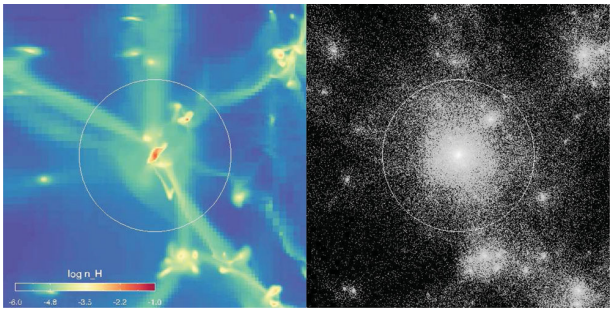

Figure 1. A typical galaxy residing in a high-mass halo ($M \sim 2 \times 10^{12}\,{\rm M}_{\odot}$ at $z = 3.8$). The radii of the circles in both the panels correspond to $R_{\rm vir} = 79\,{\rm kpc}$. Gas (left-hand panel) and dark matter (right-hand panel) projected densities are plotted. Gas filaments are significantly thinner than their dark matter counterpart. Note the extent and coherence of the large-scale gaseous filaments surrounding that galaxy.

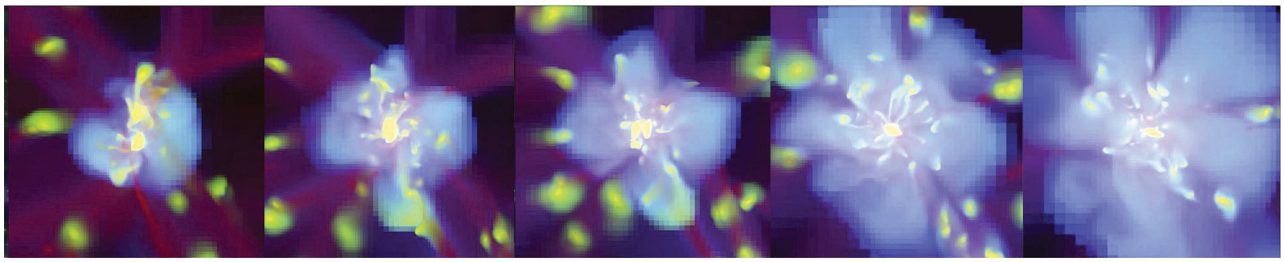

Figure 2. These panels display a time sequence representing the evolution of the halo between $z = 4$ and 2.5 colour coded with density (red), metallicity (green) and temperature (blue) within a fixed reference frame centred on the dark matter halo at all times. The consistency of the direction of the infalling gas (in red) is obvious.

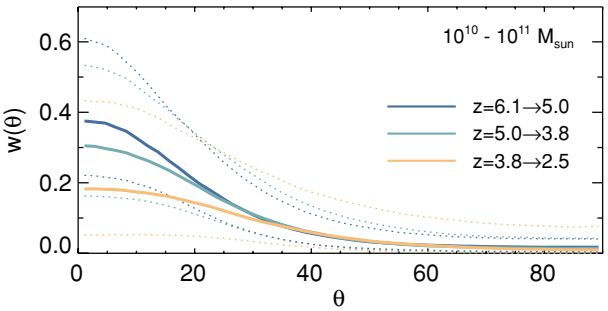

Figure 3. The covariances (thick line) between different redshifts (as labelled) of the thresholded density maps on the virial sphere, $R_{\rm vir}$, together with the corresponding dispersion (interquartile, dotted lines). The lower bound of the thresholded density is chosen such that filamentary structures stand out, while the upper bound is adopted to minimize the signal from the satellites (see the text, Section 2). The orientation of filaments is temporally coherent, as is qualitatively illustrated in Fig. 2.

The simulation yields a sample of 3119, 6655, 11 357, 15 419 and 15 999 haloes at $z = 6.1$, 5.0. 3.8, 2.5 and 1.5, respectively. This corresponds to all haloes with $M_{\rm vir} \gtrsim 2.3 \times 10^{10}\,{\rm M}_\odot$.

Let us first address the issue of consistency of the orientation of large-scale filaments that pierce the virial sphere of dark haloes.[1] Fig. 3 displays the cross-correlation of $n_{\rm H\,I}$ maps on the virial sphere, $R_{\rm vir}$, for different pairs of redshifts as labelled on the figure. This figure corresponds to the statistical average over HEALPIX (Górski et al. 2005) maps of thresholded gas density measured at $R_{\rm vir}$. Since we are primarily interested in filaments, wall-like structures and void regions are excluded by imposing a redshift-dependent threshold density. This is chosen as 6.6 times the critical density of the universe, which identifies the filamentary structures reasonably well at the resolution of the Mare Nostrum simulation. The contribution from satellite galaxies is minimized by replacing the region occupied by satellite galaxies with gas at the density threshold for star formation: $n_{\rm H} = 0.1\,{\rm cm}^{-3}$. The cross-correlation coefficient plotted is defined as

$$w(\theta) = \sum_{l,m} \langle a_{lm} b^*_{lm} \rangle P_l(\cos(\theta)) / \sqrt{\sum_{l,m} \langle |a_{lm}|^2 \rangle \sum_{l,m} \langle |b_{lm}|^2 \rangle},$$

where a_{lm} and b_{lm} are the harmonic transforms of the maps at the two given redshifts, P_l is the Legendre polynomial and $\langle\ \rangle$ stands for the statistical median over haloes within the considered mass range. The angle θ measures the separation between two pixels on the cross-correlated maps, while the cut-off frequency is $l_{\rm max} = 256$.

Fig. 3 shows that for haloes with $M \sim 10^{10}$–$10^{11}\,{\rm M}_\odot$ there is a significant correlation of the directions of the gas infall between markedly different redshifts, $w(0) \approx 0.3$–0.4 [$w(0) = 1$ implies total correlation]. This is especially true at high redshifts. Since haloes of this mass have accumulated the bulk of their matter over $\Delta z \approx 1.2$ by redshift $z \approx 3.5$, this value yields a *lower* bound on the amount of temporal coherence achieved over finer time-slices taken through the epoch of assembly of the outer regions of a galactic patch.

Let us now turn to the impact such a temporal coherence has on the advection of gas angular momentum through the virial sphere. As the accretion-weighted specific angular momentum at virial radius reads

$$\langle j \rangle_{v_r} = \left| \frac{\sum_i m_i v_r \Theta(-v_r) \boldsymbol{r}_i \times \boldsymbol{v}_i}{\sum_i m_i v_r \Theta(-v_r)} \right|, \quad (1)$$

where Θ is the Heaviside step function, we measure it by adding the contribution of the infalling[2] ($v_r < 0$) gas cells or particles within a shell with $0.95 \leq r/R_{\rm vir} \leq 1.05$. Note that $\boldsymbol{v}_i$ and $\boldsymbol{r}_i$ are measured relative to the centre of the halo and m_i is the mass of cell i. The values we quote are averages over the whole halo sample at each redshift.

Fig. 4, left-hand panel, shows that the advected angular momentum *modulus* of the gas is increasing with cosmic time and halo mass according to a trend qualitatively consistent with that expected in the spherical collapse picture (Quinn & Binney 1992). The right-hand panel represents the spin parameter ($\lambda = j/\sqrt{2} R_{\rm vir} V_{\rm c}$, Bullock et al. 2001) for the same haloes. Note that, in this definition, the virial radius, $R_{\rm vir}$, and the circular velocity, $V_{\rm c}$, are mostly set by the dark matter component. A residual trend in the evolution of gas spin as a function of redshift is clearly visible, along with larger values of $\lambda_{\rm gas}$ compared to $\lambda_{\rm DM}$. Note that, strictly speaking, $\langle \lambda \rangle_{v_r}$ is plotted for the gas in contrast to λ for the DM. However, $\langle \lambda \rangle_{v_r}$ is similar to λ for the gas component in simulations where radiative cooling is accounted for (see Kimm et al. 2011 for details) which means that the comparison is valid. This does not mean that the spin of the freshly accreted DM differs from that of the gas (it actually is very similar to what is shown in Kimm et al. 2011); rather it means that the *total* spin of the dark matter halo differs from that of the gas (see also Chen, Jing & Yoshikaw 2003; Sharma & Steinmetz 2005; Brook et al. 2011). Such an increase in the gas angular momentum as a function of cosmic time was also noticed by Brooks et al. (2009).

Fig. 5 displays the ratio of the z-component of the advected spin of the gas (where the z-axis is chosen to be aligned with the spin of the dark halo) to the modulus of that spin. The dense

[1] See Appendix A for a geometric analysis of the this effect.

[2] Note that multiple accounts of backslash is statistically subdominant.

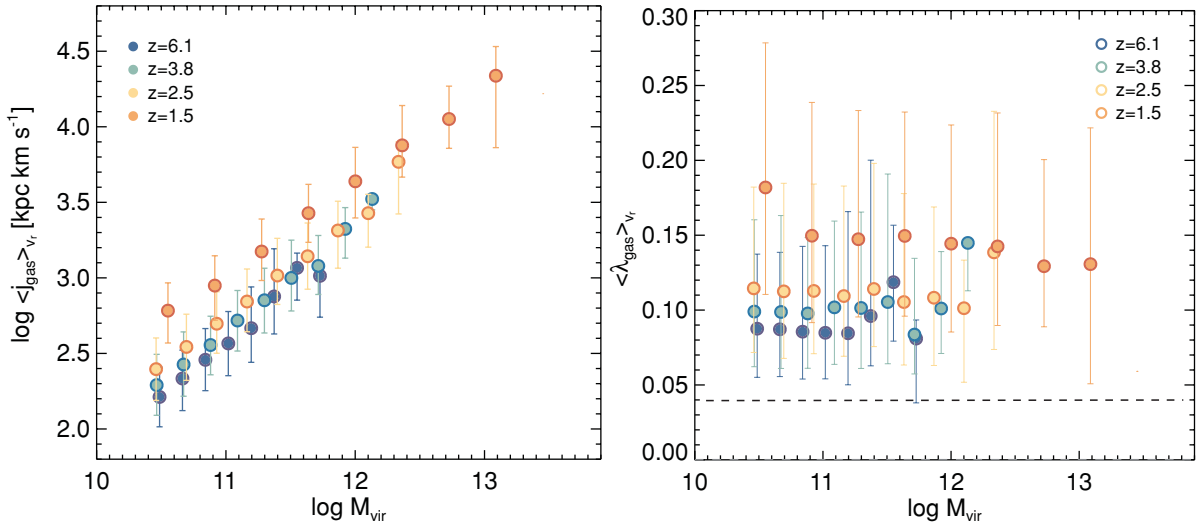

Figure 4. Left: advected specific momentum of gas as a function of cosmic time and mass in the HORIZON-MareNostrum simulation. Note that more and more gas angular momentum is being advected as a function of time and mass. Right: advected spin parameter of gas as a function of cosmic time and mass; a redshift trend persists, while the amplitude of the advected spin parameter is larger than the averaged value of 0.04 (indicated by the horizontal dashed line) measured for dark matter haloes independently of time and mass (Barnes & Efstathiou 1987; Kimm et al. 2011).

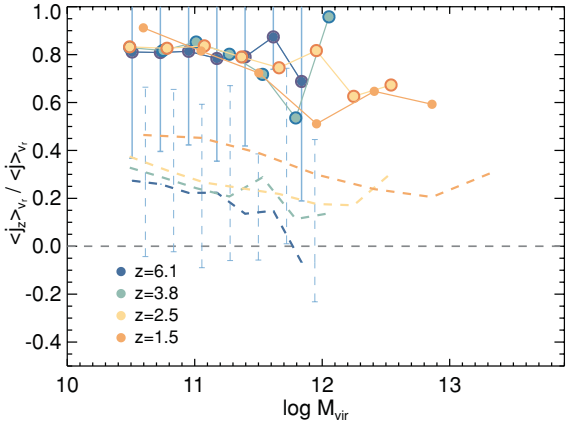

Figure 5. The ratio of the component of the spin of the advected gas along the axis defined by the spin of dark matter, to the amplitude of the spin of the advected gas, as a function of mass and redshift, for the dense (solid)/diffuse (dashed) component in the HORIZON-MareNostrum simulation. This measurement corresponds to the median of 3119, 6655, 11 357, 15 419 and 15 999 haloes, resp. for $z = 6.1$, 5.0. 3.8, 2.5 and 1.5. The cold flow is more aligned than the diffuse flow. This supports the view that the momentum-rich gas flows along the filaments and preserves most of its orientation. See Fig. 7 for a map illustrating the concentration of momentum in the filaments.

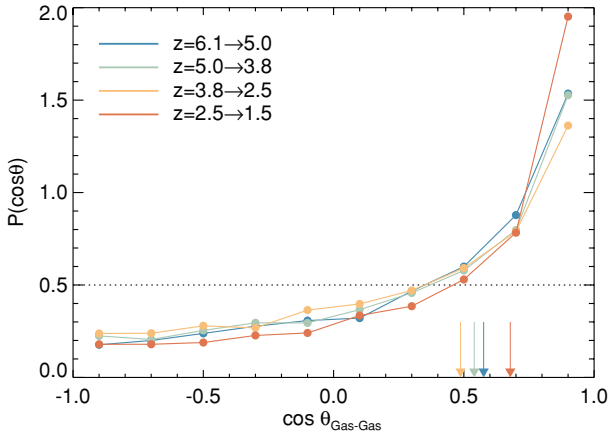

Figure 6. PDF of the cosine of relative angle between the spin of the advected gas, $\langle \boldsymbol{j} \rangle_{v_r}$, for different pairs of redshifts as labelled. The mean of this PDF is also represented as a vertical arrow for the various pairs of redshifts considered. The orientation of the spin of filaments is temporally coherent.

component of the advected (filamentary) flow (represented by the solid line) is distinguished from the diffuse material (dashed line) using the following density thresholds: $\times\ 10^{-3}$, 5×10^{-4} and $8 \times 10^{-5}\ n_{\rm H}\ {\rm cm}^{-3}$ for $z = 6.1$, 3.5 and 1.8, respectively. From the plot, it is clear that the dense infalling gas has a spin fairly well aligned with that of the dark matter whatever the mass or the redshift considered and that in any case, this denser gas arrives much more aligned than the diffuse gas at the virial radius. Note that the z-component of the *diffuse* gas increases with redshift. Fig. 7 shows examples of typical maps of λ_z and gives a good idea of the alignment of material with large values of λ_z with the main direction of the filaments. As a matter of fact, such maps are quite representative of the statistical result presented in Fig. 5.

Finally, Fig. 6 represents the probability distribution function (PDF) of the cosine of the relative angle between the advected angular momentum of the gas at different redshifts, as labelled in the plot. It quantifies the correlation of the orientation of the momentum of the infalling gas with cosmic time. If there was no change in the direction of the angular momentum vector of a filament between redshifts, this PDF would be a Dirac distribution centred on $\cos(\theta) = 1$. On the other hand, if the direction of the angular momentum vector of a filament was completely uncorrelated with redshift, the PDF would be a constant independent of $\cos(\theta)$. The fact that it is markedly peaked around $\cos(\theta) = 1$ shows that the amount of shifting/twisting/merging of filaments during cosmic time intervals is quite limited. This figure complements the

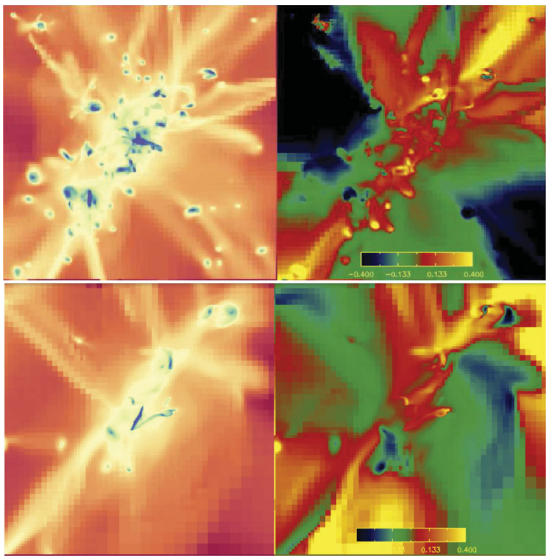

Figure 7. The distribution of the z component (i.e. along the spin axis of their dark matter halo) of the spin parameter (λ_z, right-hand panels) at $z = 3.8$ in the HORIZON-MareNostrum simulation for two different mass haloes: 5×10^{12} (top panels) and $3 \times 10^{12}\,M_\odot$(bottom panels). Projections of the hydrogen density are shown in the left-hand panels. The field of view is 4 virial radii on a side. It is apparent that some filaments display large values of λ_z (colour coded in yellow).

correlation found in Figs 2 and 3 for the orientation of the filaments themselves and corresponds, in redshift space, to the spatial correlation of the relative orientation of angular momentum along the filaments described in Appendix B.

Together, Figs 3–6 allow us to draw the following statistically robust conclusions: for the range of redshifts ($z > 1.5$) and mass considered and the corresponding subgrid physics implemented in the HORIZON-MareNostrum simulation, cold gas is advected through filaments at the virial radius with an increasing spin parameter along a consistent direction. The corresponding advected angular momentum orientation is significantly correlated with time and its orientation is consistent with that of the dark matter halo's spin. These trends are further established in a companion work (Kimm et al. 2011) which exploits much (at least a hundred times) better resolved individual galaxies in the NUT suite of zoom simulations. In that paper, it is also convincingly demonstrated that the gas within $R_{\rm vir}$ has *more* specific angular momentum than its DM counterpart. Let us now explain these statistical measurements at the virial radius through the dynamics of the surrounding cosmic web.

3 GRAVITATIONAL COLLAPSE OF GALACTIC PATCH

3.1 The origin of the angular momentum

It is now accepted that the origin of the angular momentum of galaxies is in the initial distribution of the matter velocities in the patches from which galaxies are formed. The shape of a typical protogalactic patch is neither spherically symmetric, nor bounded by equipotential surface, which results in a total (i.e. integrated over the patch) non-zero angular momentum that grows during the linear stage of structure formation due to torques on the patch from the gravitational tidal field (Peebles 1969; Doroshkevich 1970; White 1984). The angular momentum growth $\propto a^2 \dot{D}(t)$, where $D(t)$ is the growing mode of gravitational instability, extends to the non-linear Zeldovich regime (Porciani, Dekel & Hoffman 2002a,b). At this stage, the specific angular momenta of baryons and dark matter are equal. While the global properties of the following non-linear collapse of the patch are well captured by the spherical model or, with more precision, by the elliptical approximation of the peak–patch theory (Bond & Myers 1996), the detailed distribution of matter and motions in the patch are much more complex. At intermediate mildly non-linear stages, the dark matter in the patch assembles into the hierarchical cosmic web. The gas follows the potential formed by the dark matter but is subject to pressure forces whose balance determines the level at which the gas tracks the dark matter. Numerical simulations (see Fig. 1) show that the cold ($T \sim 10^4$ K) gas forms rather narrow and smooth filaments that follow the less well defined, wider and clumpier dark matter filamentary overdensities.

In this paper we intend to understand the later time infall of momentum-rich material on an early formed protohalo. The deviation of the matter motion from semiradial is especially significant in the outer layers of the patch. Let us consider a smoothed picture of the patch, with a smoothing scale, $R_{\rm smooth}$, selecting the inner halo region that collapsed at a high redshift, $z = z_{\rm in}$. An example of such a smoothed patch is shown in Fig. 8 (see Section 3.2 for details of this experiment). The exterior region contains the mass that will be accreted during further evolution to redshift $z_{\rm col} < z_{\rm in}$ by which the whole patch collapses.

The dominant features of the geometry of the outer mass distribution are filamentary bridges that emanate from the central halo and extend to the neighbouring peaks. Saddle points along the filaments mark the boundary of our patch. Calculations of the peak–saddle cross-correlations in the Gaussian initial field (Pichon et al., in preparation.) show that the typical separation between a peak and the boundary saddle is $\approx 2R_{\rm smooth}$, with little sensitivity to the power spectrum slope. Hence, our choice of the inner halo scale $R_{\rm inner} = R_{\rm smooth}$ to be half the radius of the patch $R_{\rm patch} = 2R_{\rm smooth}$ allows us to just resolve the filamentary environment of the protohalo. We relate our picture to the tidal torque theory[3] in Fig. 9 where the evolution of the angular momentum of dark matter is measured separately for the inner core and the outer envelope of a representative Milky Way like patch (the NUT simulations; see Kimm et al. 2011 for details).

While the dynamics of the smoothed inner halo can be approximated by the ellipsoidal collapse with matter infalling along mostly radial trajectories, the filaments represent structures in which the outer matter with significant transverse velocities accumulates. For this matter the velocity component parallel to the filaments is statistically reduced so the drain of matter from filaments dominates the accretion on to the inner halo at the later times. Note that the time it takes for the inner halo to collapse is similar to the time for the outer filaments of the same scale to turn around (Pogosyan et al. 1998), reaching overdensities $\delta \sim 10$ and forming potential troughs to channel cold gas.

For illustration, let us first observe the typical *initial* properties of a patch around the peak in 2D, as shown in Fig. 10.

The theory of the skeleton of the cosmic web (Novikov, Colombi & Doré 2006; Pogosyan et al. 2009) provides an approximate

[3] But, in contrast to the classical tidal torque theory (TTT) framework, we investigate the properties of our patch in greater detail, effectively using a filtering scale roughly twice as small as that used in TTT. This constitutes departure from the quadratic representation of the density and tidal fields which, we argue, is important in driving the anisotropy of the delayed infall.

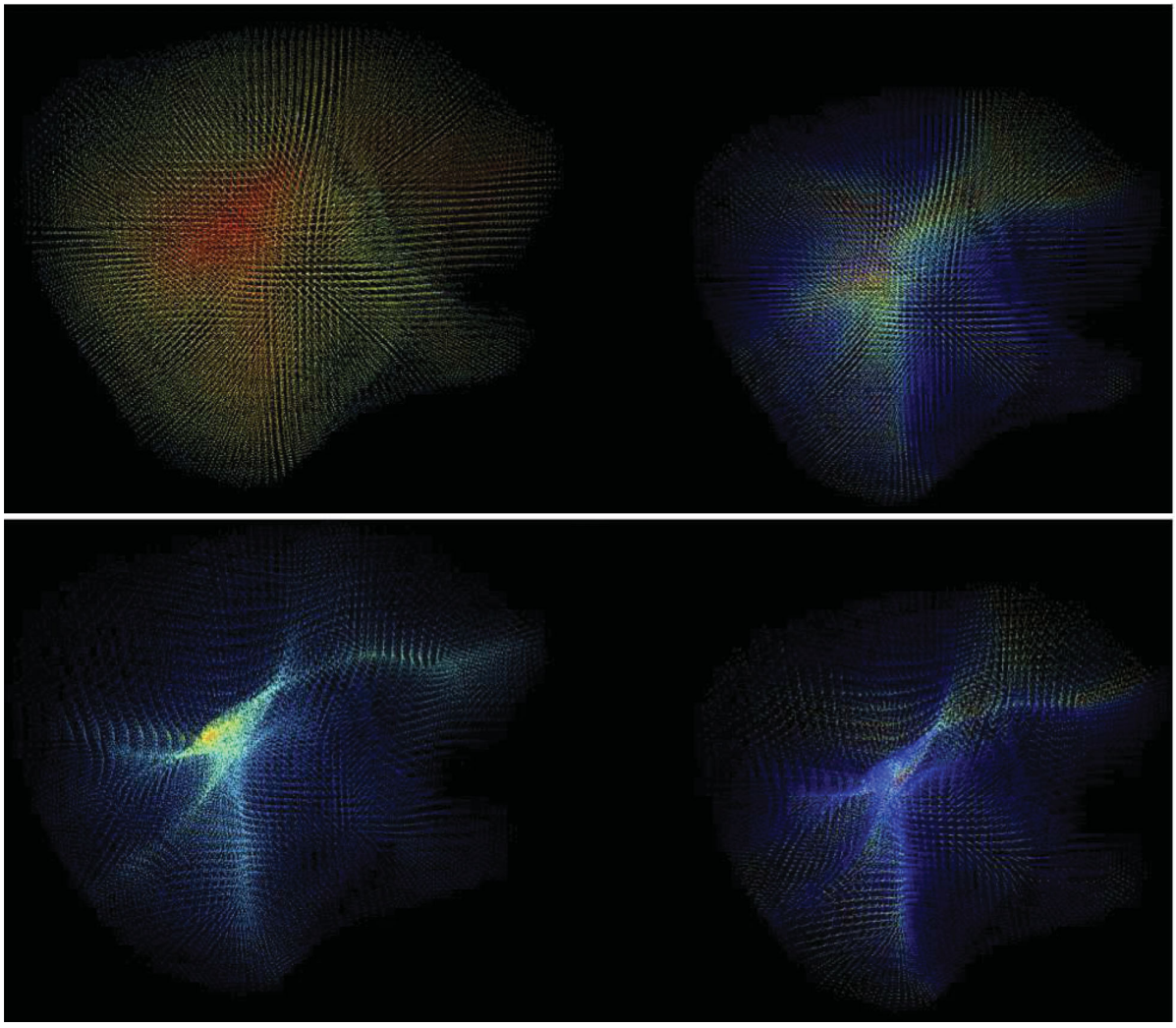

Figure 8. Colour-coded density (left-hand column) and modulus angular momentum (right-hand column) of the patch at early, $z > z_{\rm in}$, time (top row) and at the redshift of the inner halo collapse $z = z_{\rm in}$ (bottom row). This figure illustrates the structure of the angular momentum distribution and its later accretion in a collapsing (protocluster) patch with a radius of 4.7 Mpc h^{-1}. The progenitors of the filamentary structures in the initial conditions, i.e. the central halo, $\sim R_{\rm smooth} = 1.5\,{\rm Mpc}\,h^{-1}$ in size, and the filaments emanating from it, are initially momentum poor, since they are the regions where velocity is predominantly radial. The high-momentum particles (in blue) are in the voids outside (not so much at the centres of voids but closer to walls/filaments) where the velocities are more transverse with regard to the filaments. At the linear stage the structures remain unmodified, with amplitudes of velocities and, hence, angular momenta of the particles, growing, but displacement of the matter negligible. When the patch enters its non-linear dynamical stage, the high-momentum matter starts accumulating in the filaments, making the filaments the locus of momentum-rich material. Filaments change from being momentum poor to momentum rich during the time needed for the matter to travel from voids to filaments, which is similar to the time the inner halo takes to collapse. We observe that at redshift $z_{\rm in}$, exactly when the inner halo virializes, filaments have changed to their momentum-rich status. This picture also shows that it takes time $t > t_{\rm in}$ for the momentum-rich particles from the outskirts to reach the halo, since the velocity of particles parallel to the filament is statistically lower. Filaments provide momentum-rich material at the accretion stage following initial halo formation.

boundary of the collapsing patch by defining it as surfaces that pass through the saddle points on the filaments linked to the central peak. This partitioning is not exact in view of the future non-linear evolution of the structure, but is closely related to the partitioning of the initial velocity flow pointing to the peak. Importantly, it illustrates the generally non-spherical nature of the initial protohalo.

The map of the angular momentum in Fig. 10 shows that at the initial stage both the central region and primary dense filaments (the filaments that form bridges to neighbouring haloes, in our example tracked by branches 2 and 6 of the skeleton) typically contain matter with initially little angular momentum. Particles with high angular momentum are spread outside the dense structures in regions with alternating sense of rotation. As the evolution of the patch progresses, these filaments will collect the high angular momentum from the outside material and, being responsible for the late accretion towards the central peak, supply angular momentum after the central halo forms. The angular momentum in a filament is dynamically contained in the displacement of its apex with regard to the centre of the mass of the halo, and its residual transverse motion. Both are generic features of filamentary structures formed in gravitational collapse, whose relative impact may vary with the mass of the filament and the structure of the patch. Note finally that

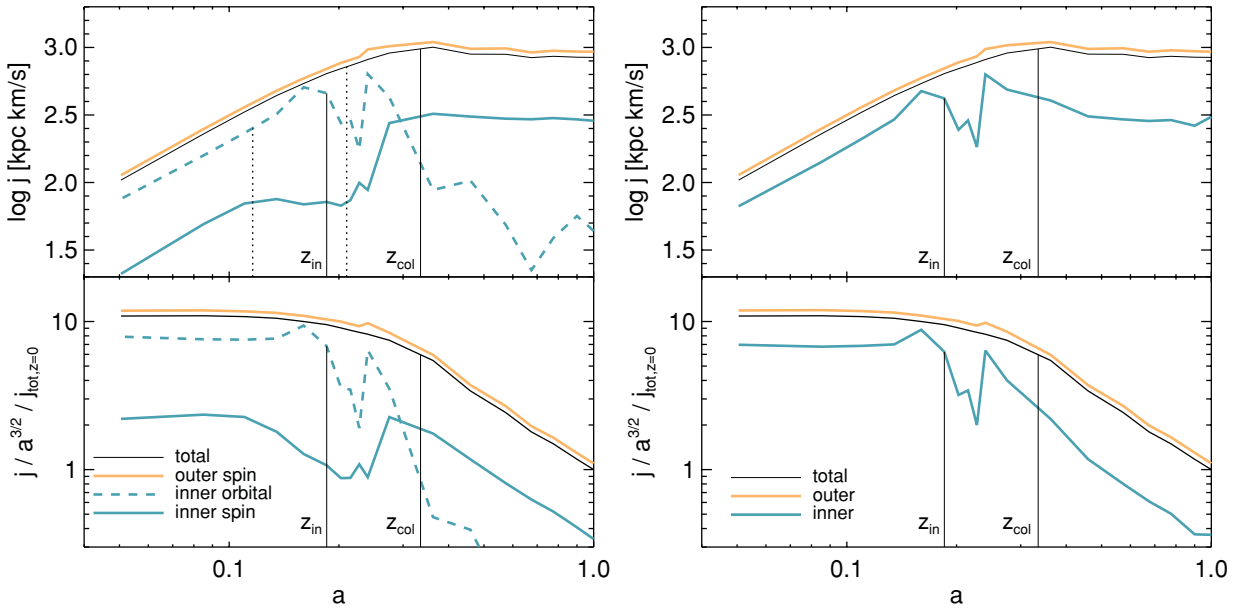

Figure 9. Evolution of the specific angular momentum in a patch of $M = 4 \times 10^{11}\,\mathrm{M}_\odot$, which is split into an inner core with $M_{\rm in} = 5 \times 10^{10}\,\mathrm{M}_\odot$ and $R_{\rm inner} \approx R_{\rm patch}/2$ and the outer envelope which contains the remaining 7/8 of the total mass. In the spherical top-hat model approximation, the patch collapses at around $z \approx 2$ which we identify with $z_{\rm col}$. The inner core is found to correspond to an independent virialized halo at $z \approx 4.4$, which is identified with $z_{\rm in}$. These redshifts are indicated by vertical solid lines in the figure. In addition, vertical dotted lines show the time of turnaround of the inner core at $z \approx 7.7$ and of the total patch at $z \approx 3.8$. It is not accidental that the outer regions turn around becoming non-linear at approximately the same time as the inner core collapses, as it follows from our selection of the inner core to have roughly half the radius of the whole patch. The upper-left plot shows the evolution of the specific angular momentum of the inner, outer and all the particles with regard to the centres of mass (CoM) of the corresponding particle sets, i.e. the spin of the total patch (thin black line), the spin of a cloud of particles in the outer region (yellow line) and the spin of the inner halo (cyan line), respectively. In addition, the orbital momentum of the inner halo with regard to the total CoM is shown as a dashed cyan line. The bottom-left plot shows the same data but divided by $a^{3/2}$, the expected scaling of the angular momentum before turnaround in TTT. We observe that the inner halo spin follows the expected behaviour, growing $\propto a^{3/2}$ until turnaround, and then remaining constant during its virialization process. At the same time the inner particles have a significant orbital momentum with regard to the total CoM, which continue to grow $\propto a^{3/2}$, essentially accounting for a Zeldovich-like motion of the inner core CoM relative to the total CoM. The situation changes when the outer envelope turns around: the orbital momentum of the inner halo is progressively converted into spin as the CoMs of the inner and large patches are brought together. By the time the whole patch collapses, the inner spin settles at the level that is enhanced, but is still below the spin of the matter located in the outer parts of the patch. The right-hand panels are similar to the left-hand ones but summarize the behaviour of the angular momentum with regard to the whole patch CoM only. It again highlights the importance of the $z_{\rm in}$-to-$z_{\rm col}$ time interval for the distribution of the angular momentum in a forming galaxy.

the amount of angular momentum cancellation expected during the crossing of shells is bound to be less important in 3D than for this oversimplified setting.

3.2 The 3D dynamics of the collapsing patch

The fate of the total angular momentum within the patch is encoded within the initial condition and the later evolution of the surrounding tidal field (Doroshkevich 1970). As a larger and larger fraction of the patch turns around, it becomes insensitive to the latter, hence its enclosed angular momentum is conserved. However, since the Vlasov–Euler–Poisson set of equations is non-linear, the detailed timing and the geometry of the flow matter in determining how and where this angular momentum is redistributed locally. In the first stage of the gravitational collapse, angular momentum is mostly in the transverse motion within the expanding voids, then it partially cancels out in walls as the void shells cross; it cancels out again in filaments, and again towards the centre along the filaments. In effect, the measured flux of momenta at various radii all depends (i) on the subtle imbalance in transverse motion which was there to start with (i.e. on the relative geometry of surrounding voids), (ii) on the relative mass in these different structures, (iii) on the external and internal torquing between these components, and finally (iv) on the fraction lost to spinning-up the substructures forming along. It is therefore not straightforward to visualize the different stages of the transport in three dimensions.

To demonstrate in 3D the development of the filamentary structure in the outer regions of a collapsing patch and its role in angular momentum transport, let us carry out the following idealized numerical experiment. We generate the initial conditions of a $100\,h^{-1}$ Mpc ΛCDM simulation using MPGRAFIC (Prunet et al. 2008) with 256^3 dark matter particles. The *initial* density and velocity cubes are then smoothed with a Gaussian filter of $\sigma = 1.5\,\mathrm{Mpc}\,h^{-1}$. The smoothed initial conditions are then run down to $z = 0$ where a Friends-of-Friends (FoF) catalogue is constructed. Within that catalogue we choose a somewhat massive halo ($\sim 2 \times 10^{14}\,\mathrm{M}_\odot$), define the halo patch as the Lagrangian extension of all particles that end up within the FoF halo at $z = 0$, and follow the evolution of these particles. The patch therefore consists of an inner core that is defined by the smoothing length and an outer envelope that develops filamentary structure which we focus upon. We stress that the only density field which we ever smooth is the initial one. Such a low-resolution simulation allows a qualitative discussion of the dark matter patch structure. Appropriate physical conditions at the correct scales and

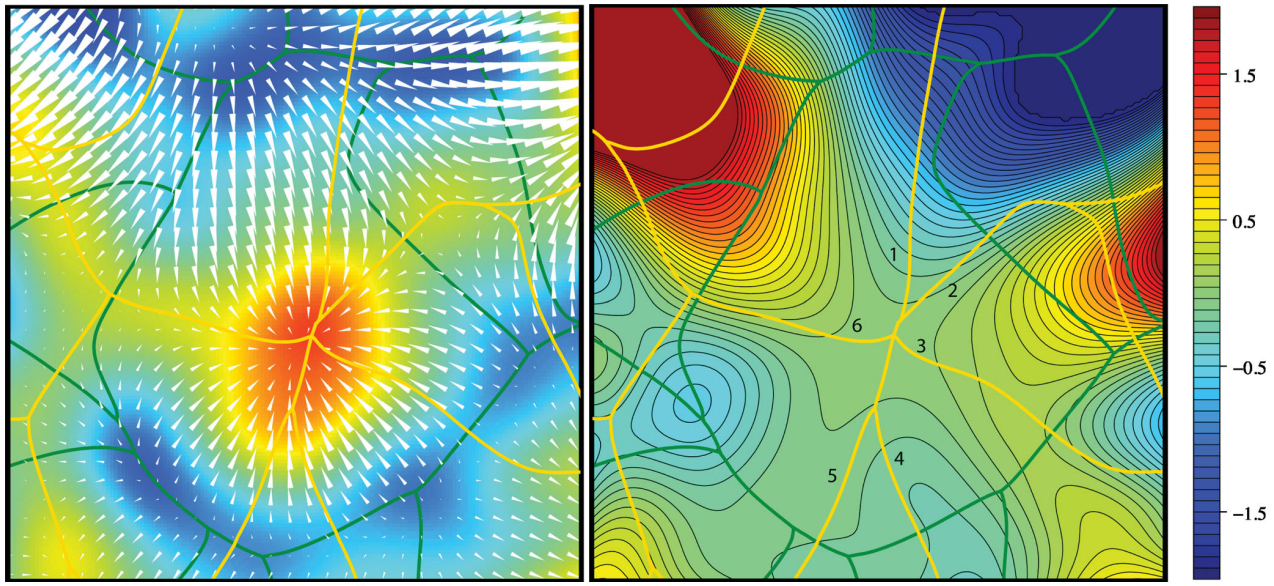

Figure 10. Left-hand panel: 2D density field and 2D initial velocity field measured with regard to the central peak. Right-hand panel: the corresponding angular momentum with regard to the central peak position. The green colour corresponds to small angular momentum as, for example, near the central peak. Both deep blue and red colours are regions of high-magnitude angular momenta, of opposite signs, clockwise and anticlockwise, respectively. In both panels the skeleton of the progenitors of the filamentary structure is superimposed as golden lines. Green lines map the boundary of the patch according to the density gradient flow. The most massive filaments (#2 and #6) to be formed are those that form overdense bridges to the neighbouring haloes. These filaments are indeed the loci of the divergence of the velocity field and are the progenitors of long-lived structures along which the matter drains on to the central halo with a time delay relative to the isotropic infall. They define the directions along which much of the outer material will reach the halo (a note of caution: one should not consider the initial velocity field as delineating flow lines for the future infall of material). In the example given, these directions are not generally coincident with the shape of the central elliptical protohalo, but are defined by the position of the neighbouring haloes and voids and the resulting velocity field structure. However, it is when there is an alignment of the peak and the shear of the velocity field that the most prominent filaments arise (Bond, Kofman & Pogosyan 1996). These dense filaments provide deep enough potentials to contain the $T \sim 10^4$ K gas. The other (e.g. #1, #3, #4 and #5) filaments of the skeleton, although mapping critical lines of the density gradient by construction, may not be associated with particularly notable overdensities. They reflect short-lived anisotropies of the collapse of the halo as, for example, might arise from a mismatch of the orientation of the original peak with the velocity flow.

redshifts need to be considered when extending the scenario to describing gaseous filaments.

Fig. 8 shows the density structure of the patch as it evolves from its initial conditions, and the distribution of angular momentum amongst the particles in the patch. While high angular momentum particles initially are found predominantly in the voids, outside the inner core and filament progenitors in the initial conditions, they aggregate to the filamentary regions, as the latter grow in density. Even with the cancelling effects of transverse shell crossing taken into account, the filaments become the locus of relatively high angular momentum by the time, $z_{\rm in}$, of inner core collapse. The angular momentum is then contained in the residual transverse motion of the filaments and their misalignment with respect to the centre of mass of the patch.

Fig. 11 displays a time sequence projection of the log-density within that patch. The filaments connecting the central halo to the edge of the patch are clearly visible, and their relative motion does reflect the tidal field within that patch. At the first stage of the gravitational collapse, both the central peak and the surrounding voids compete to, respectively, attract and repel the dark matter on the outskirts of the patch. From a distance, this figure suggests that indeed the orientation of the filaments does not change much over the course of the collapse of that patch (see also Fig. 13 below).

Fig. 12 shows the trajectories of particles colour-coded by redshift over a range of cosmic time. Inspecting these trails in 3D is instructive and led us to the scenario presented in this paper. It is quite clear that the trajectories of the dark matter particles initially within the voids of the patch present a sequence of inflections. These inflections correspond to shell crossings, when the flow either reaches a wall or a filament or finally the central peak. For instance, the right-hand panel of Fig. 12, which corresponds to a zoom of the north-east filament, presents such whirling trajectories, where a fraction of the transverse flow within the surrounding walls coils up and is converted into a spinning, sinking feature within the filament. Through this process, a fraction of the orbital angular momentum within the large-scale structure is transformed into spin, while the residual transverse motion is converted into the drift of the filament.[4] Indeed, Fig. 13 demonstrates this on the smoothed IC patch by tracing the filaments of different snapshots using the skeleton (Sousbie, Pichon & Kawahara 2011), a code that basically identifies the ridges connecting peaks and saddle points of the density field. Here the 'persistent skeleton' was computed from the dark matter particles within the patch, and co-added for a range of redshift while keeping fixed the position of the most bound particle. The residual distortion from one snapshot to another reflects the drift of the momenta-rich filaments.

[4] This cosmic flow within filaments is also consistent with the measured spin of dark haloes in filaments (Codis et al., in preparation)

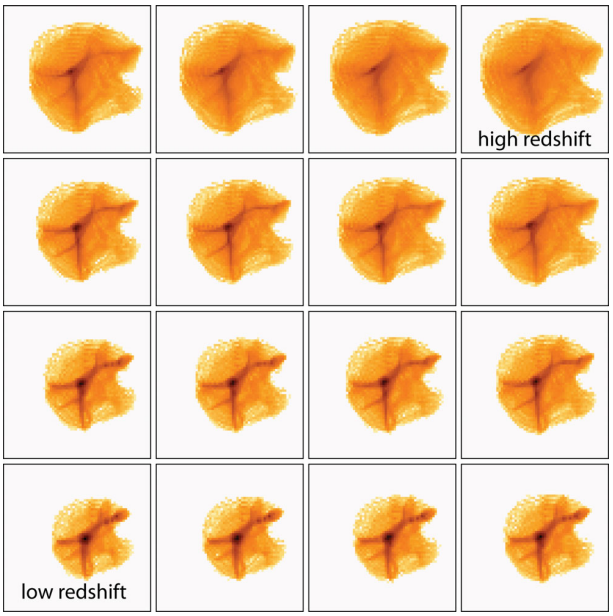

Figure 11. Projected view of the dark matter density in a collapsing patch with smoothed out ICs as a function of cosmic time from top to bottom and right to left. As these maps reflect the entire merging history of a given halo, they clearly show that the incoming direction of the infall remains fairly constant with time, with a residual drift, which reflects the advected angular momentum along the filament (see also Figs 2 and 13).

Let us now look at the actual angular momentum advected and cancelled in the flow. Fig. 14 displays the vector fields of the momenta for three snapshots, roughly corresponding to times when most of the momentum still lies in the voids (left-hand panel), a significant fraction had started migrating in the filaments and walls (middle panel), and most of the flow had converged into the central object and filaments (right-hand panel). In this figure, the colour coding reflects the amplitude of the angular momentum and spans the same range of values across the three panels. It follows that the amplitude of the advected angular momentum is lower along the filaments than in the voids (owing to the cancellation while it is being formed), but displays a significant gradient along the north and the west filament in the right-hand panel. Of course these idealized numerical experiments raise the so-called 'cloud in the cell problem': here we focus on a 'hot dark matter' picture of things where competing processes on smaller scales do not disrupt the larger scale structure of the flow. This assumption is reasonable, as we expect the larger scale distribution of matter to impact most the later angular momentum advection. The hydrodynamical results of Section 2 suggest they are not statistically dominant, at least beyond redshift[5] $z = 1.5$.

4 DISCUSSION

This paper has presented a series of results concerning the nature of the angular-momentum-rich dynamical gas flows at the virial radius of collapsed dark matter haloes. Measurements were carried out using the AMR Mare Nostrum simulation (Ocvirk et al. 2008), which allowed us to draw the following conclusions: at redshift 1.5 and above, gas inflow through the virial sphere is focused (preferred inflow direction), consistent (orientation of advected angular momentum steady in time), and amplified (increasing amplitude of advected angular momentum as time passes). The qualitative analysis of very simple 2D initial conditions and idealized dark matter simulations have allowed us to explain this coherent flow in terms of the dynamics of the corresponding gravitational patch.

4.1 Advection of angular momentum along cold flows

In view of these findings we sketched the following scenario for the gas flow along cold streams. On the outskirts of a forming halo, large-scale flows arise as the surrounding voids expel gas and dark matter. As the flows coming from opposite directions meet, dark matter undergoes shell-crossing whilst the gas shocks, cools and collapses into the newly created walls and filaments at the boundary between voids. Each of these boundaries acquires a net transverse velocity which reflects the asymmetry between the voids it divides. Within the boundary, the longitudinal component of the flow then drags gas towards the growing halo, advecting angular momentum in the process. As the transverse velocity should be similar along the boundary, the later the infall on to the halo, the further it originates from, the larger the angular momentum it brings (lever effect). Thus the orientation of the advected angular momentum at the virial radius of the halo is steady in time, as it is piloted by this large-scale transverse motion which in effect is encoded in the initial conditions of the patch. It also means that gas hits the virial sphere of the halo along a preferred direction: that of the incoming filaments/walls.

We are now in a position to try and answer the two questions raised in Section 1, namely 'how and why is gas accreted on to the galactic disc?'. The answer to the 'how' is: by building up the circumgalactic medium through the direct accretion of cold gas with an ever-increasing and (fairly well) aligned angular momentum. The answer to the 'why' is: because the internal dynamics of the cosmic web within the peak patch produces such a coherent flow. Angular-momentum-rich inflow is delayed compared to radial inflow as a fraction of the patch first flows away from voids into the walls and filaments. Only then is this material brought back to the direction of the halo.

Hence the anisotropic distribution of angular momentum outside of the collapsed halo is critical to explaining the *formation* of thin galactic discs. It means that the gas arrives at $R_{\rm vir}$ in two distinct flavours, dense versus diffuse, as outcomes of different dynamical histories within the peak patch. The denser phase is produced as gas collapses into the walls and filaments where it cools and which further feed the central halo. The diffuse phase is either the gas that is accreted directly on to the halo, or the hot gas that was unable to cool due to low density, and was not confined to filamentary structures. As the result, the hot gas does not display a preferred alignment with regard to the dark halo's spin (Fig. 5), as this coherence is only achieved via filamentary infall in which it did not participate. Even though the mass involved in filamentary flows can be small compared to the total gas mass involved in the formation of the central galaxy at any given time, it should play a critical role in supplying the circumgalactic region constructively with increasingly angular-momentum-rich gas, while at the same time minimizing the destructive impact of incoming substructures on the existing disc. In short, in this scenario discs are in fact *produced by*, rather than *shielded from*, the cosmic environment.

[5] Substructures on smaller scales may become relevant at lower redshifts when dark energy kicks in and dries out the gas supply, for a subset of massive haloes embedding elliptical galaxies (see Domínguez-Tenreiro et al. 2010 and the discussion below).

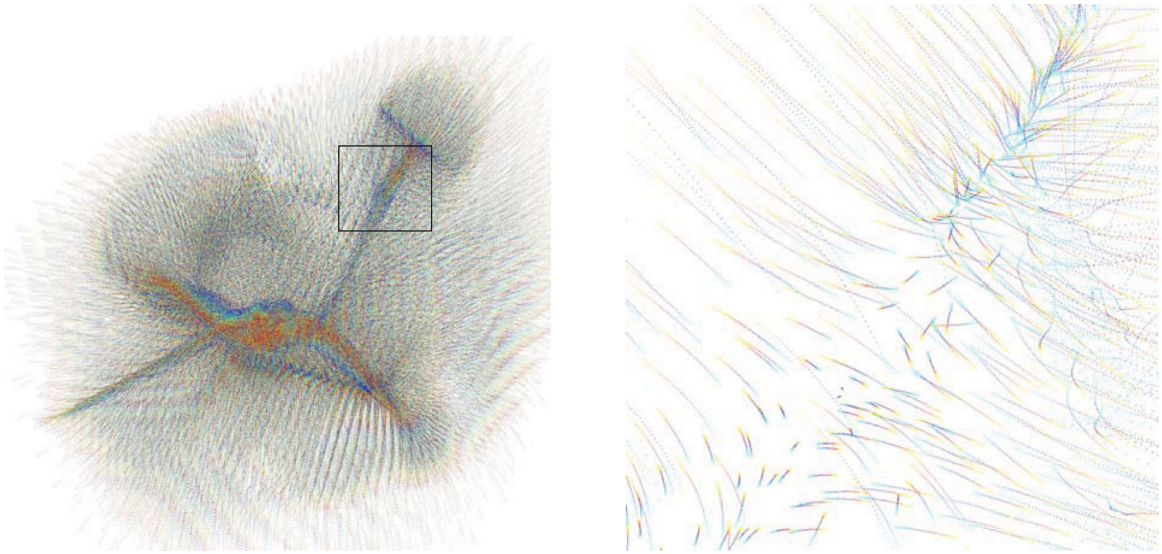

Figure 12. Left: example of trajectories of dark matter particles, colour coded by redshift from red (high redshift) to blue (low redshift). These trails first converge towards the filaments and then along the filaments towards the central halo: their motion account for both the orbital angular momentum of the filamentary flow and the spin of satellites formed within those filaments. Right: a zoom of the left-hand panel corresponding to the shell-crossing between two walls leading to the formation of the north-east filament. Some of the angular momentum lost in the transverse motion is given to the spin of structures forming within that filament; the rest is converted into the angular momentum of the filament. The corresponding animation is available for download at http://www.iap.fr/users/pichon/rig/.

4.2 The dynamics of the gas within $R_{\rm vir}$

Though the dynamics of the infalling gas within $R_{\rm vir}$ is complex and is the topic of companion papers (Kimm et al. 2011; Powell et al. 2011; Tillson et al., in preparation), we qualitatively describe here what happens to the cold gas brought by filamentary streams into $R_{\rm vir}$ as it reaches the outskirts of the central disc (the circumgalactic medium). Simulations show that these filaments penetrate the $\sim R_{\rm vir}/10$ region on an infalling orbit, while roughly preserving their radial velocity and width (Dekel et al. 2009), radiating away the kinetic energy acquired during the free fall (Goerdt et al. 2010). They typically overshoot the centre of the halo until they encounter the counterfalling diffuse gas against which they radiatively shock (Powell et al. 2011) and resume their plunging orbit, which is a much less radial orbit progressively spiralling in towards the inner disc.

A limited loss of the coherence inherited from the large-scale structure is expected to occur: as the filamentary inflow has a geometry which is steady in time, so should the shock. Similarly, the gravitational interaction between infalling satellites and the existing triaxial halo and pre-existing protodisc should only have a time-limited impact on the reshuffling of angular momentum within that region. In a nutshell, we expect the consistency of the cosmic flow to overcome, in the long run, the occasionally messy circumgalactic environment of forming discs. Using the NUT (Powell et al. 2011, see below) suite of highly resolved hydrodynamical simulations, Kimm et al. (2011) find that the specific angular momentum of the gas is at least twice as large as that of the dark matter in the DM halo, $R_{\rm vir}/10 < r < R_{\rm vir}$ (see also e.g. Chen et al. 2003; Sharma & Steinmetz 2005; Stewart et al. 2011). More importantly they find that this specific angular momentum is, most of the time, well aligned with that of the central galactic disc region. This means that the outer halo region acts like a reservoir of rapidly spinning cold gas, which coherently builds the disc inside out. We therefore conjecture that, at least *statistically*, disc galaxies owe the survival of their thin disc to the consistency of the cosmic infall.

4.3 Linking the gas flow within a disc galaxy to its large scale structure filamentary origin above redshift 1.5

To substantiate the view that the gas angular momentum of galaxies is preferentially advected along filaments and naturally leads to the inside-out build-up of thin discs throughout cosmic ages, we make use of a high-resolution hydrodynamical simulation in the NUT suite (Powell et al. 2011). The ultimate goal of the NUT suite is to quantify the effect of various physical mechanisms (cooling, supernovae/AGN feedback, magnetic fields, radiative transfer) on the properties of well-resolved galaxies (several grid cells spanning the scaleheight of the disc) embedded in their cosmological environment. To achieve this objective, a cubic volume of the Universe 12.5 comoving Mpc on a side with periodic boundary conditions is tiled with a uniform 128^3 coarse grid. Within this volume, an initial high-resolution sphere (1024^3 equivalent) of about 1 Mpc in radius is defined which encompasses the Lagrangian region from which the dark matter particles of a Milky Way size halo at $z = 0$ originate. As the simulation progresses, up to 10 additional levels of grid refinement are triggered in a quasi-Lagrangian manner so as to keep the size of the smallest grid cell equal to 12 physical pc at all times. The initial conditions of the simulation were generated using MPGRAFIC (Prunet et al. 2008) and adopting a *WMAP5* cosmology with $\Omega_{\rm m} = 0.258$, $\Omega_\Lambda = 0.742$, $h \equiv H_0/(100\,{\rm km\,s^{-1}\,Mpc^{-1}}) = 0.72$ (Dunkley et al. 2009). This yields a dark matter particle mass of $\simeq 5.5 \times 10^4\,{\rm M}_\odot$ in the high-resolution region. The simulation includes radiative cooling, star formation and a uniform redshift-dependent UV background instantaneously turned on at $z = 8.5$ (Haardt & Madau 1996). The gas density threshold for star formation is chosen to be equal to the Jeans threshold,

Figure 13. The sweeping skeleton within the inner region of the patch shown in Fig. 11 colour coded by redshift from dark (high z) to light (low z). The central peak is in the middle of the figure. To zeroth order, this figure suggests that the direction of the filament does not change much. Looking more closely, from one redshift to another, the various branches of the skeleton do slide with cosmic time. Indeed, the net transverse motion following shells crossing of the filament will induce a residual drift of the filament, which the skeleton captures. At the top of this plot, note the top left-most fork before a satellite which will merge with the central halo at a later time.

i.e. $n_{\rm H,th} = 400\,{\rm cm}^{-3}$ The minimal mass of star particles is therefore $\simeq 2 \times 10^4\,{\rm M}_\odot$.

We then track the evolution of the gas flow in our Eulerian grid simulation using tracer particles. These are massless particles whose initial positions and number exactly match those of the DM particles in the simulation. However, as the simulation proceeds, they are simply advected with the local velocity of the gas calculated by means of a Cloud-in-Cell interpolation. Fig. 15 shows such gas tracing particles in the NUT simulation at $z = 6.5$, painted in a different colour depending on which concentric spherical shell they belong to (top-left panel). These spherical shells are centred on the disc galaxy and they do not overlap. The background image is a projection of the underlying gas temperature. Note that most of the tracer particles are associated with the cold gas component, consistent with the result of Powell et al. (2011) that the galactic gas growth in mass at high redshifts is dominated by cold filamentary accretion (see also Appendix A). The position of these coloured particles then is displayed at redshifts $z = 8.5$ and 11.5 in the top-middle and top-right panels, illustrating that their radial ordering is preserved over significant periods of time. The bottom-right, bottom-middle and bottom-left panels present line graphs of the radii of these particles and their angular momenta at $z = 8.5$ and 11.5 respectively. Notwithstanding the fact that the NUT simulation only follows the first Gyr of the evolution of a galaxy, it is clear from Fig. 15 that, as we have argued in this paper, (i) the origin of the cold gas in the disc and its neighbourhood is filamentary, (ii) outer shells of gas come from outer regions which carry more angular momentum, and (iii) the angular momentum of accreted gas increases with cosmic time.

4.4 Extensions and perspectives for low-redshift discs?

In this paper, the emphasis was put on the inflow from the cosmic environment on to galactic discs. More specifically, we have addressed the implication of angular momentum transport by cold flows from large scales down to the virial radii of the dark haloes hosting these central disc galaxies.

In doing so, we deliberately overlooked several important issues. First, our work has noticeably ignored the well-documented dichotomy between galaxies located in dark matter haloes above and below the critical halo mass for shock stability (Kereš et al. 2005; Dekel & Birnboim 2006; Ocvirk et al. 2008; Brooks et al.

Figure 14. Redshift sequence ($z > z_{\rm in}$, $= z_{\rm in}$ and $< z_{\rm in}$) displaying the 3D angular momentum vector field, colour-coded by amplitude (with the same dynamical range throughout; dark corresponds to large angular momentum, light to intermediate angular momentum; low angular momentum is not shown). Note that the choice of colour is arbitrary and is only dictated by the requirement that the colour be different for different redshift bins. The left-hand panel clearly shows that the voids are angular momentum rich, the middle panel shows that near $z_{\rm in}$ the filaments have partially advected (and partially cancelled out) a fair fraction of the void's momenta, while the right-hand panel shows that the remaining angular momentum indeed is carried in through the filaments. Note that the region of high and intermediate momenta do not overlap much between $z > z_{\rm in}$ and $< z_{\rm in}$, as expected given the flow. The corresponding density is displayed in Figs 7 and 10 along different orientations. A rough estimate gives that filaments, walls and voids contain 60, 30, 10 per cent of the specific angular momentum at $z = z_{\rm in}$. The corresponding animation is available online at http://www.iap.fr/users/pichon/rig/.

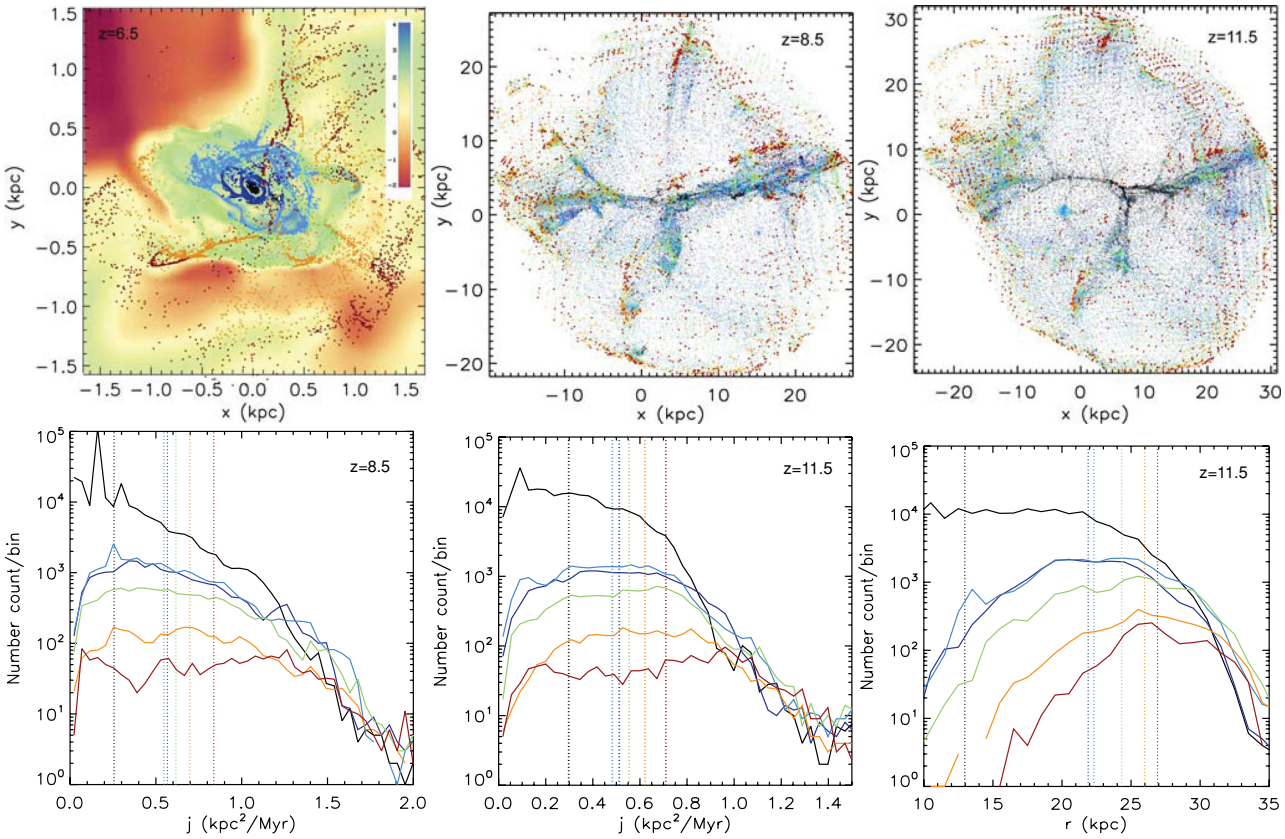

Figure 15. The position of the tracer particles superimposed on the gas temperature at redshift $z = 6.5$ (top-left panel), and the positions of the tracer particles at $z = 8.5$ (top-middle panel) and $z = 11.5$ (top-right panel). The different colours (black, dark blue, light blue, green, orange, red) for the tracer particles only encode information about their radial position at $z = 6.5$ (the concentric, non-overlapping spherical shells they belong to). Note how well the tracer particles follow the shocks and prefer the cold phase. The (bottom-left panel) shows line graphs of the particles' angular momenta at $z = 8.5$ (bottom-left panel), $z = 11.5$ (bottom-middle panel) and radii (bottom-right panel) (the vertical dashed line represents the mean of each PDF). The progenitor of the different annuli around the disc is clearly found in the earlier filaments, while the stratification is consistent with an inside-out build-up of the circumgalactic medium. As expected, the angular momentum of tracer particles increases with cosmic time.

2009). The mass accretion process in these two galaxy populations is known to be thermodynamically (cold versus hot mode) and geometrically (connected to multiple filaments or embedded in them) different and also to depend sensitively on redshift, to the point that even the relevance of cold flows at low redshifts (below $z = 1.5$) has been questioned. The simulations carried out in this paper did not address the angular momentum content of the corresponding possibly quasi-spherical hot gas accretion. Secondly, feedback processes internal to the central galaxies (massive stars, supernovae, AGN) may reduce the relevance of anisotropic infall as they may partially isotropize outflows, which, in turn, could lead to a disruption of the inflow. Third, along with the cold gas, the cosmic inflow will advect galaxy/dark halo satellites. The relative fraction of induced minor/major, dry/wet merger will certainly affect the Hubble type of the central object even though the 'cosmic' consistency of the accretion reported in this paper should have a statistical bearing on the preferred direction of satellite infall at $z = 0$ (Deason et al. 2011). As discussed in Section 4.2, the dynamics *within* the virial radius of the dark matter host halo is also bound to be significantly more complex: the shorter dynamical time, dynamical friction and tidal stripping of satellites, torquing from the central triaxial halo and radiative shocking should introduce a non-negligible amount of angular momentum redistribution for the gas within the circumgalactic region.

In a recent paper, Domínguez-Tenreiro et al. (2010), guided by smoothed particle hydrodynamics (SPH) cosmological simulations, address the mass assembly of massive *ellipticals* in the framework of the adhesion model (Gurbatov, Saichev & Shandarin 1989; Kofman, Pogosian & Shandarin 1990). In accordance with this scenario, they also trace back the origin of star-forming gas to neighbouring cold filaments (cf. Section 4.3). On the other hand, they also find that hot intrahalo gas originates from diffuse regions where strong shell crossing is yet to occur. As their focus is on the progenitors of massive galaxies, which would correspond to rounder (Pichon & Bernardeau 1999) peak patches associated with rarer events, they measure very little angular momentum advection in the first stage of the collapse. As we are concerned with less massive, more common disc-like galaxies, the associated initial density peak is more ellipsoidal and an early angular momentum advection is therefore more important.

The extension of TTT to quantify the amount of angular momentum *expected* to be acquired after $z_{\rm in}$ constitutes a natural follow-up of the current paper. Such a theory could be constructed from a higher resolution description of the density field in the patch

(i.e. which includes features such as ridges and saddle points that appear when the patch is smoothed on scales smaller than its ellipsoidal representation via the inertial tensor), using theoretical tools such as the skeleton (Pogosyan et al. 2009). Such an extension involves predicting the relative dynamical importance of the different filaments embedded within the patch, both in terms of advected mass and angular momentum. One expects that the six filaments typically connected to a given 3D peak (Pichon et al., in preparation) mostly cancel each other out in terms of net angular momentum flux as all the voids surrounding a given peak cannot induce rotation along the same axis. This extension will need to account for the filamentary bifurcations (e.g. Pogosyan et al. 2009) inside the peak patch in order to see why only two prevail eventually. One would then be able to possibly predict *ab initio* a fraction of the cosmic history of galactic spin-up. Such a theory for the rigging of dark haloes should be within reach, and will be the topic of further investigation.

ACKNOWLEDGMENTS

We thank J. Binney, S. Codis, A. Dekel, M. Haehnelt, J. Magorrian, S. Peirani, S. Prunet and J. F. Sygnet for useful comments during the course of this work, and the referee for his suggestions. CP acknowledges support from a Leverhulme visiting professorship at the Department of Physics, University of Oxford, and thanks Merton College, Oxford, for a visiting fellowship, and Lena for her hospitality. DP thanks the French Canada Research Fund. TK acknowledges support from a Clarendon DPhil studentship. JD and AS's research is supported by Adrian Beecroft, the Oxford Martin School and STFC. YD is supported by an STFC Postdoctoral Fellowship. We also acknowledge support from the Franco-Korean PHC STAR programme and the France Canada Research Fund. The HORIZON-MareNostrum simulation was run on the MareNostrum machine at the Barcelona Supercomputing Centre and we would like to warmly thank the staff for their support and hospitality. The NUT simulation presented here was run on the DiRAC facility jointly funded by STFC, the Large Facilities Capital Fund of BIS and the University of Oxford. This research is a part of the Horizon & Horizon-UK project. Let us thank D. Munro for freely distributing his YORICK programming language and the OPENGL interface (available at http://yorick.sourceforge.net/), J. Patterson and S. Rouberol for their constant help and T. Sousbie for the persistent skeleton code DISPERSE.

REFERENCES

Aubert D., Pichon C., Colombi S., 2004, MNRAS, 352, 376
Barnes J., Efstathiou G., 1987, ApJ, 319, 575
Benson A. J., Bower R., 2011, MNRAS, 410, 2653
Bertschinger E., 1985, ApJS, 58, 1
Binney J., 1977, ApJ, 215, 483
Birnboim Y., Dekel A., 2003, MNRAS, 345, 349
Bond J. R., Myers S. T., 1996, ApJS, 103, 1
Bond J. R., Kofman L., Pogosyan D., 1996, Nat, 380, 603
Brook C. B., Stinson G., Gibson B. K., Roškar R., Wadsley J., Quinn T., 2011, MNRAS, doi:10.1111/j.1365-2966.2011.19640.x
Brooks A. M., Governato F., Quinn T., Brook C. B., Wadsley J., 2009, ApJ, 694, 396
Bullock J. S., Dekel A., Kolatt T. S., Kravtsov A. V., Klypin A. A., Porciani C., Primack J. R., 2001, ApJ, 555, 240
Chen D. N., Jing Y. P., Yoshikaw K., 2003, ApJ, 597, 35
Deason A. J. et al., 2011, MNRAS, 415, 2607
Dekel A., Birnboim Y., 2006, MNRAS, 368, 2
Dekel A. et al., 2009, Nat, 457, 451
Devriendt J. et al., 2010, MNRAS, 403, L84
Domínguez-Tenreiro R., Oñorbe J., Martínez-Serrano F., Serna A., 2010, preprint (arXiv: 1010.6294)
Doroshkevich A. G., 1970, Astrophysics, 6, 320
Dubois Y., Teyssier R., 2008, A&A, 477, 79
Dunkley J. et al., 2009, ApJ, 701, 1804
Fall S. M., Efstathiou G., 1980, MNRAS, 193, 189
Fardal M. A., Katz N., Gardner J. P., Hernquist L., Weinberg D. H., Davé R., 2001, ApJ, 562, 605
Fillmore J. A., Goldreich P., 1984, ApJ, 281, 1
Goerdt T., Dekel A., Sternberg A., Ceverino D., Teyssier R., Primack J. R., 2010, MNRAS, 407, 613
Górski K. M., Hivon E., Banday A. J., Wandelt B. D., Hansen F. K., Reinecke M., Bartelmann M., 2005, ApJ, 622, 759
Gurbatov S. N., Saichev A. I., Shandarin S. F., 1989, MNRAS, 236, 385
Haardt F., Madau P., 1996, ApJ, 461, 20
Katz N., Keres D., Dave R., Weinberg D. H., 2003, in Rosenberg J. L., Putman M. E., eds, Astrophys. Space Sci. Libr., Vol. 281, The IGM/Galaxy Connection. The Distribution of Baryons at $z = 0$. astro-ph/0209279
Kay S. T., Pearce F. R., Jenkins A., Frenk C. S., White S. D. M., Thomas P. A., Couchman H. M. P., 2000, MNRAS, 316, 374
Kereš D., Katz N., Weinberg D. H., Davé R., 2005, MNRAS, 363, 2
Kereš D., Katz N., Fardal M., Davé R., Weinberg D. H., 2009, MNRAS, 395, 160
Kimm T., Devriendt J., Slyz A., Pichon C., Kassin S. A., Dubois Y., 2011, MNRAS, submitted (arXiv:1106.0538)
Kofman L., Pogosian D., Shandarin S., 1990, MNRAS, 242, 200
Mo H. J., Mao S., White S. D. M., 1998, MNRAS, 295, 319
Novikov D., Colombi S., Doré O., 2006, MNRAS, 366, 1201
Ocvirk P., Pichon C., Teyssier R., 2008, MNRAS, 390, 1326
Peebles P. J. E., 1969, ApJ, 155, 393
Pichon C., Bernardeau F., 1999, A&A, 343, 663
Pogosyan D., Bond J. R., Kofman L., Wadsley J., 1998, in Colombi S., Mellier Y., Raban B., eds, Proc. 14th IAP Meeting, Wide Field Surveys in Cosmology Cosmic Web: Origin and Observables. Editions Frontieres, Gif-sur-Yvette, p. 61
Pogosyan D., Pichon C., Gay C., Prunet S., Cardoso J. F., Sousbie T., Colombi S., 2009, MNRAS, 396, 635
Porciani C., Dekel A., Hoffman Y., 2002a, MNRAS, 332, 325
Porciani C., Dekel A., Hoffman Y., 2002b, MNRAS, 332, 339
Powell L. C., Slyz A., Devriendt J., 2011, MNRAS, 414, 3671
Prunet S., Pichon C., Aubert D., Pogosyan D., Teyssier R., Gottloeber S., 2008, ApJS, 178, 179
Quinn T., Binney J., 1992, MNRAS, 255, 729
Rees M. J., Ostriker J. P., 1977, MNRAS, 179, 541
Sharma S., Steinmetz M., 2005, ApJ, 628, 21
Silk J., 1977, ApJ, 211, 638
Sousbie T., Colombi S., Pichon C., 2009, MNRAS, 393, 457
Sousbie T., Pichon C., Kawahara H., 2011, MNRAS, 414, 384
Stewart K. R., Kaufmann T., Bullock J. S., Barton E. J., Maller A. H., Diemand J., Wadsley J., 2011, ApJ, 738, 39
Sutherland R. S., Dopita M. A., 1993, ApJS, 88, 253
Teyssier R., 2002, A&A, 385, 337
White S. D. M., 1984, ApJ, 286, 38

APPENDIX A: GEOMETRY OF GAS ACCRETION

The scenario proposed in Section 3 is based on the assumption that cold filamentary accretion primarily accounts for the growth of the central gaseous disc at high redshifts. This has been studied by several authors (e.g. Brooks et al. 2009; Kimm et al. 2011). In this section, we aim to provide further statistical evidence for the geometrical nature of the infall by looking at the power spectrum of gas accretion from the HORIZON-MareNostrum simulation.

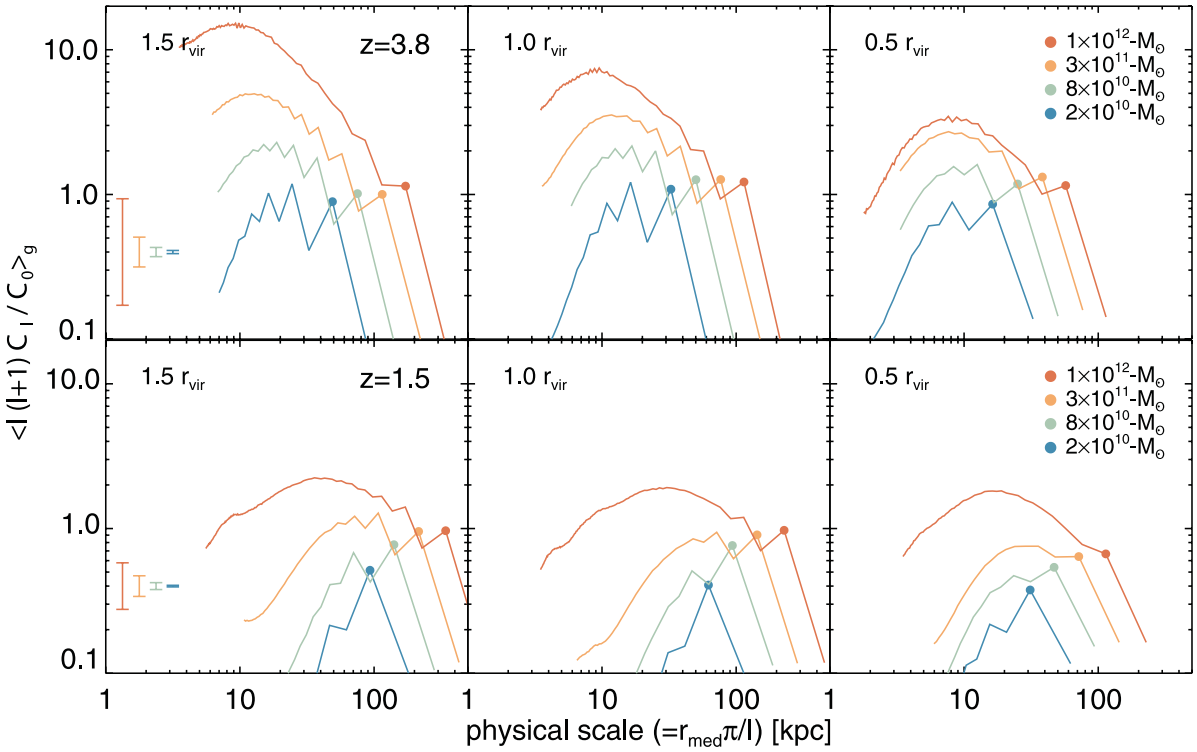

Figure A1. Normalized power spectrum of gas accretion at different radii. The ordinate indicates the geometric mean of the power spectrum, normalized by the monopole (C_0), and abscissa indicates the physical scale ($\equiv r_{\rm med}\pi/l$) corresponding to each multipole (l). The median radius ($r_{\rm med}$) of each subsample is used to compute the physical scale. Different colour-coding denotes different halo mass bins, and the quadrupole ($l = 2$) is marked as a filled circle. Power spectra for high ($z = 3.8$) and low redshift ($z = 1.5$) are shown in the upper and lower panels, respectively. The radius at which the power spectrum is measured decreases from left to right. Error bars in the left-hand panels are the maximum standard errors of the mean in each mass bin. The most massive haloes ($M_{\rm vir} > 10^{13}\,{\rm M}_{\odot}$) are not included in this analysis because of their small number. This figure shows that statistically, the advected gas is coming along filaments whose cross-section increases with cosmic time and for lighter haloes.

We make use of the HEALPIX package (Górski et al. 2005) to transform accretion maps into power spectra, $l(l + 1)C_l$, with the tessellation parameter NSIDE = 128. We first divide the sample by halo mass and compute the average power spectra for each mass bin. We average the power spectra normalized by the monopole term, i.e. $\langle l(l + 1)C_l/C_0\rangle_g$, where $\langle\ \rangle_g$ denotes the geometrical mean (in order to properly account for the typically lognormal distribution of the different power spectra of individual haloes). Note that C_0 represents the global accretion rate, and hence the power normalized by C_0 corresponds to the relative contribution from each mode l. In order to account for the limited resolution of the simulation, the measurement of the power spectra for modes greater than $l_{\rm lim} \equiv \pi\Delta x_{\rm min}/r$ are discarded, where $\Delta x_{\rm min}$ is the minimum size of the AMR cell used to obtain the map, and r is the radius of the corresponding spherical shell.

Fig. A1 shows the power spectrum of the gas accretion as a function of the *physical scales* corresponding to each harmonic multipoles at $z = 3.8$ (upper panels). The virial radii vary with halo mass, so each multipole does not correspond to the same physical size for all dark matter haloes. Thus, we use the median radius of each subsample $r_{\rm med}\pi/l$, to investigate the physical scale of the accretion. We plot the results when more than 95 per cent of the haloes show a reliable estimate of the power spectrum. This induces a cut-off of $\simeq$2–10 kpc depending on halo mass.

We find that the characteristic scale of gas accretion (corresponding to the peak of the power spectra) is around 10–30 kpc at $z = 3.8$, which is roughly the scale of filaments in Fig. 1. This supports the view that gas accretion is mainly filamentary at high redshifts. At a lower redshift ($z = 1.5$) one expects that the filaments become more diffuse and broader as the universe expands. This view is borne out by the bottom panels of Fig. A1 which suggest that the characteristic size of the accretion is $\sim$60 kpc at the virial radius for $z = 1.5$. In particular, for less massive haloes ($M_{\rm vir} \leq 5 \times 10^{11}\,{\rm M}_{\odot}$) that are likely to end up forming spiral galaxies, the power spectrum is dominated by the dipole term, implying that two filaments are responsible for the accretion. It is worth noting that at larger distances ($r = 1.5\,r_{\rm vir}$) the characteristic scale becomes larger than the diameter of $5 \times 10^{10}\,{\rm M}_{\odot}$ haloes ($\sim$80 kpc), indicating that smaller haloes are probably embedded within the filament(s).

An interesting feature of Fig. A1 is the oscillation in the power spectra. Such an oscillating power spectrum at *low* multipoles can be found when the contribution from even modes is superior to that from odd modes. The preference for even modes indicates that gas accretion is dominated by an even number of sources, which are likely to be separated by $\sim\pi$ on the sky. If the accretion were dominated by one strong source, i.e. a satellite galaxy, the power spectrum for odd modes would be larger than that for even modes and the oscillatory feature would vanish or be reversed. However, it should be noted that the larger contribution from even modes does not necessarily mean that any even number of infalling structures will produce the same signal. Only when the contribution from such structures is significantly larger than that from other sources and

when these structures are separated by $\sim\pi$ does the power spectrum show this oscillatory feature. Note finally that the oscillatory feature turns out to be more significant for less massive haloes, suggesting again that the accretion is highly likely to be bipolar for these haloes.

APPENDIX B: ANGULAR MOMENTUM ORIENTATION CORRELATION ALONG FILAMENTS

In Section 2 we found that the orientation of advected angular momentum was fairly stationary with regard to cosmic time. Let us underpin this measurement by investigating the coherence of this orientation along the large-scale structure filaments. Consider a set of filaments (defined here as a set of segments of the skeleton between two peaks; see Sousbie, Colombi & Pichon 2009). Let s_i and s_j be the curvilinear coordinates along that filament of two segments and $\Delta\theta_{ij}$ be the relative angle of the two angular momenta, $\boldsymbol{J}_i$ and $\boldsymbol{J}_j$ separated by $s_i - s_j$ [i.e. $\cos(\Delta\theta_{ij}) = \boldsymbol{J}_i \cdot \boldsymbol{J}_i / |J_i||J_j|$]. Let us define the expectation, $\langle\cos(\theta)\rangle(r)$, of the relative angle between the angular momentum orientation as a function of distance along the filament:

$$\langle\cos(\theta)\rangle(r) = \sum_{i,j|\ |s_i - s_j| = r \pm \Delta r} \cos(\Delta\theta_{ij}) \Big/ \sum_{i,j|\ |s_i - s_j| = r \pm \Delta r} 1\,,$$

where the summation is over all pairs, i, j belonging to the same filament for which the separation in curvilinear coordinate falls within Δr of r. The average of this expectation over all filaments in the simulations is shown in Fig. B1 for the skeleton of a dark matter simulation of 256^3 particles in a cube of volume $(50\,\mathrm{Mpc}\,h^{-1})^3$ smoothed over a $1\,\mathrm{Mpc}\,h^{-1}$ scale. The orientation of the spin of dark matter particles is clearly correlated over scales of the order of $10\,\mathrm{Mpc}\,h^{-1}$. This result is qualitatively consistent with the temporal correlation of Fig. 6.

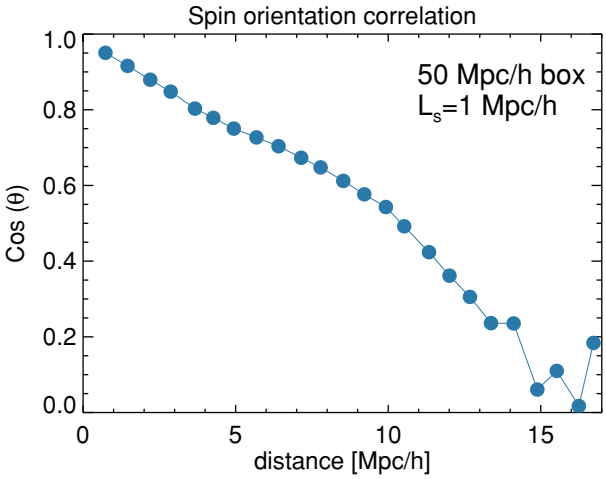

Figure B1. Expectation of the relative orientation of the angular momentum of the filamentary flow as a function of the separation along the filament; this quantity is found to be quite stable with regard to redshift.

This paper has been typeset from a TEX/LATEX file prepared by the author.